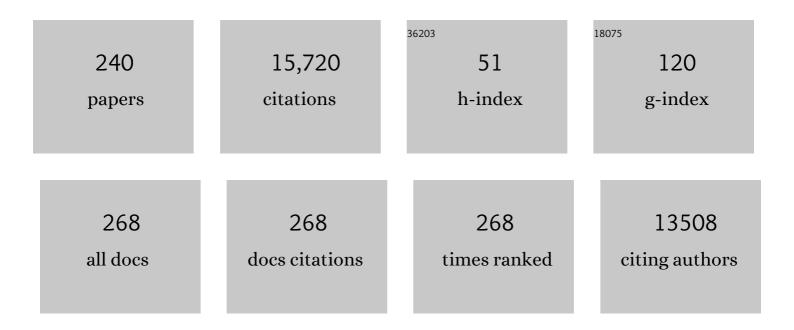
Jan Peter Muller

List of Publications by Year in descending order

Source: https://exaly.com/author-pdf/4826453/publications.pdf Version: 2024-02-01



#	Article	IF	CITATIONS
1	First operational BRDF, albedo nadir reflectance products from MODIS. Remote Sensing of Environment, 2002, 83, 135-148.	4.6	2,022
2	The Moderate Resolution Imaging Spectroradiometer (MODIS): land remote sensing for global change research. IEEE Transactions on Geoscience and Remote Sensing, 1998, 36, 1228-1249.	2.7	1,178
3	Multi-angle Imaging SpectroRadiometer (MISR) instrument description and experiment overview. IEEE Transactions on Geoscience and Remote Sensing, 1998, 36, 1072-1087.	2.7	855
4	A Habitable Fluvio-Lacustrine Environment at Yellowknife Bay, Gale Crater, Mars. Science, 2014, 343, 1242777.	6.0	687
5	Mineralogy of a Mudstone at Yellowknife Bay, Gale Crater, Mars. Science, 2014, 343, 1243480.	6.0	508
6	Mapping regional economic activity from night-time light satellite imagery. Ecological Economics, 2006, 57, 75-92.	2.9	501
7	Mars' Surface Radiation Environment Measured with the Mars Science Laboratory's Curiosity Rover. Science, 2014, 343, 1244797.	6.0	475
8	Volatile, Isotope, and Organic Analysis of Martian Fines with the Mars Curiosity Rover. Science, 2013, 341, 1238937.	6.0	367
9	Night-time Imagery as a Tool for Global Mapping of Socioeconomic Parameters and Greenhouse Gas Emissions. Ambio, 2000, 29, 157-162.	2.8	366
10	Terrestrial remote sensing science and algorithms planned for EOS/MODIS. International Journal of Remote Sensing, 1994, 15, 3587-3620.	1.3	333
11	X-ray Diffraction Results from Mars Science Laboratory: Mineralogy of Rocknest at Gale Crater. Science, 2013, 341, 1238932.	6.0	327
12	Abundance and Isotopic Composition of Gases in the Martian Atmosphere from the Curiosity Rover. Science, 2013, 341, 263-266.	6.0	327
13	Martian Fluvial Conglomerates at Gale Crater. Science, 2013, 340, 1068-1072.	6.0	326
14	Volatile and Organic Compositions of Sedimentary Rocks in Yellowknife Bay, Gale Crater, Mars. Science, 2014, 343, 1245267.	6.0	323
15	Curiosity at Gale Crater, Mars: Characterization and Analysis of the Rocknest Sand Shadow. Science, 2013, 341, 1239505.	6.0	280
16	Global retrieval of bidirectional reflectance and albedo over land from EOS MODIS and MISR data: Theory and algorithm. Journal of Geophysical Research, 1997, 102, 17143-17161.	3.3	274
17	Elemental Geochemistry of Sedimentary Rocks at Yellowknife Bay, Gale Crater, Mars. Science, 2014, 343, 1244734.	6.0	246
18	In Situ Radiometric and Exposure Age Dating of the Martian Surface. Science, 2014, 343, 1247166.	6.0	224

#	Article	IF	CITATIONS
19	Soil Diversity and Hydration as Observed by ChemCam at Gale Crater, Mars. Science, 2013, 341, 1238670.	6.0	215
20	Comparison of precipitable water vapor derived from radiosonde, GPS, and Moderate-Resolution Imaging Spectroradiometer measurements. Journal of Geophysical Research, 2003, 108, .	3.3	209
21	New Directions in Earth Observing: Scientific Applications ofMultiangle Remote Sensing. Bulletin of the American Meteorological Society, 1999, 80, 2209-2228.	1.7	204
22	Evidence from the Mars Express High Resolution Stereo Camera for a frozen sea close to Mars' equator. Nature, 2005, 434, 352-356.	13.7	201
23	Operational retrieval of cloud-top heights using MISR data. IEEE Transactions on Geoscience and Remote Sensing, 2002, 40, 1532-1540.	2.7	166
24	Interaction of eddies and mean zonal flow on Jupiter as inferred from Voyager 1 and 2 images. Journal of Geophysical Research, 1981, 86, 8733-8743.	3.3	163
25	The value of multiangle measurements for retrieving structurally and radiatively consistent properties of clouds, aerosols, and surfaces. Remote Sensing of Environment, 2005, 97, 495-518.	4.6	159
26	Moist convection as an energy source for the large-scale motions in Jupiter's atmosphere. Nature, 2000, 403, 630-632.	13.7	155
27	Interferometric synthetic aperture radar (InSAR) atmospheric correction: GPS, Moderate Resolution Imaging Spectroradiometer (MODIS), and InSAR integration. Journal of Geophysical Research, 2005, 110,	3.3	146
28	The Petrochemistry of Jake_M: A Martian Mugearite. Science, 2013, 341, 1239463.	6.0	134
29	Evaluating sub-pixel offset techniques as an alternative to D-InSAR for monitoring episodic landslide movements in vegetated terrain. Remote Sensing of Environment, 2014, 147, 133-144.	4.6	134
30	MISR stereoscopic image matchers: techniques and results. IEEE Transactions on Geoscience and Remote Sensing, 2002, 40, 1547-1559.	2.7	121
31	Interferometric synthetic aperture radar atmospheric correction: GPS topography-dependent turbulence model. Journal of Geophysical Research, 2006, 111, n/a-n/a.	3.3	120
32	Using advanced InSAR time series techniques to monitor landslide movements in Badong of the Three Gorges region, China. International Journal of Applied Earth Observation and Geoinformation, 2013, 21, 253-264.	1.4	105
33	Automated Crater Detection, A New Tool for Mars Cartography and Chronology. Photogrammetric Engineering and Remote Sensing, 2005, 71, 1205-1217.	0.3	103
34	Low Upper Limit to Methane Abundance on Mars. Science, 2013, 342, 355-357.	6.0	103
35	A Comparison of Satellite-Derived Spectral Albedos to Ground-Based Broadband Albedo Measurements Modeled to Satellite Spatial Scale for a Semidesert Landscape. Remote Sensing of Environment, 2000, 74, 85-98.	4.6	102
36	Development of a graph-based approach for building detection. Image and Vision Computing, 1999, 17, 3-14.	2.7	100

#	Article	IF	CITATIONS
37	Sampling the surface bidirectional reflectance distribution function (BRDF): 1. Evaluation of current and future satellite sensors. International Journal of Remote Sensing, 1994, 8, 271-311.	1.1	90
38	Assessment of the potential of MERIS nearâ€infrared water vapour products to correct ASAR interferometric measurements. International Journal of Remote Sensing, 2006, 27, 349-365.	1.3	83
39	Evaluation of ASTER GDEM using GPS benchmarks and SRTM in China. International Journal of Remote Sensing, 2013, 34, 1744-1771.	1.3	82
40	Interferometric synthetic aperture radar atmospheric correction: Medium Resolution Imaging Spectrometer and Advanced Synthetic Aperture Radar integration. Geophysical Research Letters, 2006, 33, .	1.5	78
41	Evaluating planetary digital terrain models—The HRSC DTM test. Planetary and Space Science, 2007, 55, 2173-2191.	0.9	69
42	How much CO was emitted by the 2010 fires around Moscow?. Atmospheric Chemistry and Physics, 2013, 13, 4737-4747.	1.9	66
43	Selection of the landing site in Isidis Planitia of Mars probe Beagle 2. Journal of Geophysical Research, 2003, 108, 1-1.	3.3	65
44	Quantifying geological processes on Mars—Results of the high resolution stereo camera (HRSC) on Mars express. Planetary and Space Science, 2015, 112, 53-97.	0.9	63
45	HRSC on Mars Express – Photogrammetric and Cartographic Research. Photogrammetric Engineering and Remote Sensing, 2005, 71, 1153-1166.	0.3	60
46	Digital Elevation Models: Terminology and Definitions. Remote Sensing, 2021, 13, 3581.	1.8	59
47	Surface movements of emplaced lava flows measured by synthetic aperture radar interferometry. Journal of Geophysical Research, 2001, 106, 11293-11313.	3.3	58
48	A refined chronology of catastrophic outflow events in Ares Vallis, Mars. Earth and Planetary Science Letters, 2009, 288, 58-69.	1.8	57
49	Late Noachian to Hesperian climate change on Mars: Evidence of episodic warming from transient crater lakes near Ares Vallis. Journal of Geophysical Research, 2010, 115, .	3.3	57
50	Fluorescence Characterization of Clinically-Important Bacteria. PLoS ONE, 2013, 8, e75270.	1.1	56
51	Laser-Induced Fluorescence Emission (L.I.F.E.): Searching for Mars Organics with a UV-Enhanced PanCam. Astrobiology, 2009, 9, 953-964.	1.5	55
52	CloudFCN: Accurate and Robust Cloud Detection for Satellite Imagery with Deep Learning. Remote Sensing, 2019, 11, 2312.	1.8	55
53	Measurements of wind vectors, eddy momentum transports, and energy conversions in Jupiter's atmosphere from Voyager 1 images. Geophysical Research Letters, 1980, 7, 1-4.	1.5	52
54	Penetrators for in situ subsurface investigations of Europa. Advances in Space Research, 2011, 48, 725-742.	1.2	51

#	Article	IF	CITATIONS
55	Measuring forests with dual wavelength lidar: A simulation study over topography. Agricultural and Forest Meteorology, 2012, 161, 123-133.	1.9	50
56	Monitoring of Eyjafjallajökull volcanic aerosol by the new European Skynet Radiometers (ESR) network. Atmospheric Environment, 2012, 48, 33-45.	1.9	50
57	Comparison of cloud top heights derived from MISR stereo and MODIS CO2-slicing. Geophysical Research Letters, 2002, 29, 42-1-42-4.	1.5	49
58	Multi-resolution topographic data extraction from Martian stereo imagery. Planetary and Space Science, 2009, 57, 2095-2112.	0.9	49
59	Degradation of Cyanobacterial Biosignatures by Ionizing Radiation. Astrobiology, 2011, 11, 997-1016.	1.5	48
60	Topographic effects in AVHRR NDVI data. Remote Sensing of Environment, 1995, 54, 223-232.	4.6	47
61	Comparison between active sensor and radiosonde cloud boundaries over the ARM Southern Great Plains site. Journal of Geophysical Research, 2003, 108, .	3.3	46
62	Stereo cloudâ€ŧop heights and cloud fraction retrieval from ATSRâ€2. International Journal of Remote Sensing, 2007, 28, 1921-1938.	1.3	46
63	Assessment of MISR and MODIS cloud top heights through inter-comparison with a back-scattering lidar at SIRTA. Geophysical Research Letters, 2004, 31, .	1.5	45
64	Sorted stone circles in Elysium Planitia, Mars: Implications for recent martian climate. Icarus, 2009, 200, 30-38.	1.1	45
65	Accurate geometric correction of ATSR images. IEEE Transactions on Geoscience and Remote Sensing, 1997, 35, 997-1006.	2.7	44
66	Digital elevation model production by stereo-matching spot image-pairs: a comparison of algorithms. Image and Vision Computing, 1989, 7, 95-101.	2.7	42
67	Intercomparison of multiple years of MODIS, MISR and radar cloud-top heights. Annales Geophysicae, 2005, 23, 2415-2424.	0.6	42
68	Context for the ESA ExoMars rover: the Panoramic Camera (PanCam) instrument. International Journal of Astrobiology, 2006, 5, 269-275.	0.9	41
69	Hesperian equatorial thermokarst lakes in Ares Vallis as evidence for transient warm conditions on Mars. Geology, 2010, 38, 71-74.	2.0	37
70	A New Global fAPAR and LAI Dataset Derived from Optimal Albedo Estimates: Comparison with MODIS Products. Remote Sensing, 2016, 8, 275.	1.8	34
71	Jovian cloud structure and velocity fields. Nature, 1979, 280, 776-778.	13.7	33
72	A threshold insensitive method for locating the forest canopy top with waveform lidar. Remote Sensing of Environment, 2011, 115, 3286-3297.	4.6	33

Jan Peter Muller

#	Article	IF	CITATIONS
73	Evaluation of the Use of Sub-Pixel Offset Tracking Techniques to Monitor Landslides in Densely Vegetated Steeply Sloped Areas. Remote Sensing, 2016, 8, 659.	1.8	33
74	Massive stereo-based DTM production for Mars on cloud computers. Planetary and Space Science, 2018, 154, 30-58.	0.9	33
75	Dynamical features in the northern hemisphere of Saturn from Voyager 1 images. Nature, 1982, 297, 132-134.	13.7	30
76	Retreat of a giant cataract in a long-lived (3.7–2.6 Ga) martian outflow channel. Geology, 2010, 38, 791-794.	2.0	30
77	Characterizing the Spatial Variability of Broadband Albedo in a Semidesert Environment for MODIS Validation. Remote Sensing of Environment, 2000, 74, 58-68.	4.6	28
78	Constraints on the origin and evolution of Iani Chaos, Mars. Journal of Geophysical Research, 2011, 116, .	3.3	28
79	Experimental determination of photostability and fluorescenceâ€based detection of PAHs on the Martian surface. Meteoritics and Planetary Science, 2012, 47, 806-819.	0.7	28
80	Geological Analysis of Martian Roverâ€Đerived Digital Outcrop Models Using the 3â€Đ Visualization Tool, Planetary Robotics 3â€Đ Viewer—PRo3D. Earth and Space Science, 2018, 5, 285-307.	1.1	28
81	Convective growth rates of equatorial features in the jovian atmosphere. Nature, 1982, 295, 491-494.	13.7	27
82	An assessment of surface matching for the automated co-registration of MOLA, HRSC and HiRISE DTMs. Earth and Planetary Science Letters, 2010, 294, 520-533.	1.8	27
83	The origin of Phobos' grooves and crater chains. Planetary and Space Science, 1994, 42, 519-526.	0.9	25
84	The importance of surface reflectance anisotropy for cloud and NO ₂ retrievals from GOME-2 and OMI. Atmospheric Measurement Techniques, 2018, 11, 4509-4529.	1.2	25
85	Voyager observations of small-scale waves in the equatorial region of the jovian atmosphere. Nature, 1979, 280, 778-780.	13.7	24
86	Deriving albedo maps for HAPEX-Sahel from ASAS data using kernel-driven BRDF models. Hydrology and Earth System Sciences, 1999, 3, 1-11.	1.9	24
87	Potential Applications of Thermal Fisheye Imagery in Urban Environments. IEEE Geoscience and Remote Sensing Letters, 2007, 4, 56-59.	1.4	24
88	Automated localisation of Mars rovers using co-registered HiRISE-CTX-HRSC orthorectified images and wide baseline Navcam orthorectified mosaics. Icarus, 2016, 280, 139-157.	1.1	24
89	A novel method for surface exploration: Super-resolution restoration of Mars repeat-pass orbital imagery. Planetary and Space Science, 2016, 121, 103-114.	0.9	23
90	Estimating land surface albedo in the HAPEX-Sahel southern super-site: inversion of two BRDF models against multiple angle ASAS images. Journal of Hydrology, 1997, 188-189, 749-778.	2.3	22

#	Article	IF	CITATIONS
91	Progressively weighted affine adaptive correlation matching for quasi-dense 3D reconstruction. Pattern Recognition, 2012, 45, 3795-3809.	5.1	22
92	Automated Stereo Retrieval of Smoke Plume Injection Heights and Retrieval of Smoke Plume Masks From AATSR and Their Assessment With CALIPSO and MISR. IEEE Transactions on Geoscience and Remote Sensing, 2014, 52, 1249-1258.	2.7	22
93	Late-stage water eruptions from Ascraeus Mons volcano, Mars: Implications for its structure and history. Earth and Planetary Science Letters, 2010, 294, 479-491.	1.8	21
94	Intercomparison of Surface Albedo Retrievals from MISR, MODIS, CGLS Using Tower and Upscaled Tower Measurements. Remote Sensing, 2019, 11, 644.	1.8	21
95	Quality Assurance Framework Development Based on Six New ECV Data Products to Enhance User Confidence for Climate Applications. Remote Sensing, 2018, 10, 1254.	1.8	20
96	Toward a Comprehensive Dam Monitoring: On-Site and Remote-Retrieved Forcing Factors and Resulting Displacements (GNSS and PS–InSAR). Remote Sensing, 2021, 13, 1543.	1.8	20
97	Time Series Analysis of Very Slow Landslides in the Three Gorges Region through Small Baseline SAR Offset Tracking. Remote Sensing, 2017, 9, 1314.	1.8	19
98	Evaluation of a CCD-based facial measurement system. Medical Informatics = Medecine Et Informatique, 1991, 16, 213-228.	0.8	18
99	Potential for nonâ€destructive astrochemistry using the ExoMars PanCam. Geophysical Research Letters, 2008, 35, .	1.5	18
100	Mapping Medusae Fossae Formation materials in the southern highlands of Mars. Icarus, 2010, 209, 405-415.	1.1	18
101	Assessment of MISR Cloud Motion Vectors (CMVs) Relative to GOES and MODIS Atmospheric Motion Vectors (AMVs). Journal of Applied Meteorology and Climatology, 2017, 56, 555-572.	0.6	18
102	Hyperspectral Features of Oil-Polluted Sea Ice and the Response to the Contamination Area Fraction. Sensors, 2018, 18, 234.	2.1	18
103	On the status of orbital high-resolution repeat imaging of Mars for the observation of dynamic surface processes. Planetary and Space Science, 2015, 117, 207-222.	0.9	17
104	The Application of ALOS/PALSAR InSAR to Measure Subsurface Penetration Depths in Deserts. Remote Sensing, 2017, 9, 638.	1.8	17
105	Single Image Super-Resolution Restoration of TGO CaSSIS Colour Images: Demonstration with Perseverance Rover Landing Site and Mars Science Targets. Remote Sensing, 2021, 13, 1777.	1.8	17
106	A study on the applicability of repeatâ€pass SAR interferometry for generating DEMs over several Indian test sites. International Journal of Remote Sensing, 2006, 27, 595-616.	1.3	16
107	ALBEDOMAP: MERIS land surface albedo retrieval using data fusion with MODIS BRDF and its validation using contemporaneous EO and in situ data products. , 2007, , .		16
108	A regional investigation of urban land-use change for potential landslide hazard assessment in the Three Gorges Reservoir Area, People's Republic of China: Zigui to Wanzhou. International Journal of Remote Sensing, 2013, 34, 2983-3011.	1.3	15

#	Article	IF	CITATIONS
109	A New South Polar Digital Terrain Model of Mars from the High-Resolution Stereo Camera (HRSC) onboard the ESA Mars Express. Planetary and Space Science, 2019, 174, 43-55.	0.9	15
110	Sea Ice Albedo from MISR and MODIS: Production, Validation, and Trend Analysis. Remote Sensing, 2019, 11, 9.	1.8	15
111	QUALITY ASSESSMENT OF DIGITAL ELEVATION MODELS PRODUCED BY AUTOMATIC STEREOMATCHERS FROM SPOT IMAGE PAIRS. Photogrammetric Record, 1988, 12, 797-808.	0.4	14
112	Tree and building detection in dense urban environments using automated processing of IKONOS image and LiDAR data. International Journal of Remote Sensing, 2011, 32, 2245-2273.	1.3	14
113	Hydraulic modeling of a distributary channel of Athabasca Valles, Mars, using a highâ€resolution digital terrain model. Journal of Geophysical Research, 2012, 117, .	3.3	14
114	On Mars too expect macroweather. Geophysical Research Letters, 2014, 41, 7694-7700.	1.5	14
115	Can We Use Satellite-Based FAPAR to Detect Drought?. Sensors, 2019, 19, 3662.	2.1	14
116	Validation of Space-Based Albedo Products from Upscaled Tower-Based Measurements Over Heterogeneous and Homogeneous Landscapes. Remote Sensing, 2020, 12, 833.	1.8	14
117	Automated urban area building extraction from high resolution stereo imagery. Image and Vision Computing, 1996, 14, 115-130.	2.7	13
118	On the use of ICESAT-GLAS measurements for MODIS and SEVIRI cloud-top height accuracy assessment. Geophysical Research Letters, 2005, 32, n/a-n/a.	1.5	13
119	A new quality validation of global digital elevation models freely available in China. Survey Review, 2016, 48, 409-420.	0.7	13
120	Super-Resolution Restoration of MISR Images Using the UCL MAGiGAN System. Remote Sensing, 2019, 11, 52.	1.8	13
121	EVALUATION OF ASTER GDEM VER2 USING GPS MEASUREMENTS AND SRTM VER4.1 IN CHINA. ISPRS Annals of the Photogrammetry, Remote Sensing and Spatial Information Sciences, 0, I-4, 181-186.	0.0	13
122	Cloud detection from thermal infrared images using a segmentation technique. International Journal of Remote Sensing, 1996, 17, 2845-2856.	1.3	12
123	Determination of phytoplankton abundances (Chlorophyll- a) in the optically complex inland water - The Baltic Sea. Science of the Total Environment, 2017, 601-602, 1060-1074.	3.9	12
124	Identification of the Beagle 2 lander on Mars. Royal Society Open Science, 2017, 4, 170785.	1.1	12
125	Rapid Single Image-Based DTM Estimation from ExoMars TGO CaSSIS Images Using Generative Adversarial U-Nets. Remote Sensing, 2021, 13, 2877.	1.8	12
126	ATSRâ€⊋ camera models for the automated stereo photogrammetric retrieval of cloudâ€ŧop heights—initial assessments. International Journal of Remote Sensing, 2007, 28, 1939-1955.	1.3	11

#	Article	IF	CITATIONS
127	The ESA globAlbedo project: Algorithm. , 2012, , .		11
128	A branching, positive relief network in the middle member of the Medusae Fossae Formation, equatorial Mars—Evidence for sapping?. Planetary and Space Science, 2013, 85, 142-163.	0.9	11
129	Mars' atmosphere: The sister planet, our statistical twin. Journal of Geophysical Research D: Atmospheres, 2016, 121, 11,968.	1.2	11
130	A New Method for Automatically Tracing Englacial Layers from MCoRDS Data in NW Greenland. Remote Sensing, 2018, 10, 43.	1.8	11
131	Ultra-High-Resolution 1 m/pixel CaSSIS DTM Using Super-Resolution Restoration and Shape-from-Shading: Demonstration over Oxia Planum on Mars. Remote Sensing, 2021, 13, 2185.	1.8	11
132	THE DIGITAL ELEVATION MODEL INTERCOMPARISON EXPERIMENT DEMIX, A COMMUNITY-BASED APPROACH AT GLOBAL DEM BENCHMARKING. International Archives of the Photogrammetry, Remote Sensing and Spatial Information Sciences - ISPRS Archives, 0, XLIII-B4-2021, 395-400.	0.2	11
133	Determination of cloud top amount and altitude at high latitudes. Geophysical Research Letters, 2001, 28, 1675-1678.	1.5	10
134	Comparison between ATSRâ€2 stereo, MOS O2â€A band and groundâ€based cloud top heights. International Journal of Remote Sensing, 2007, 28, 1969-1987.	1.3	10
135	A Systematic Solution to Multi-Instrument Coregistration of High-Resolution Planetary Images to an Orthorectified Baseline. IEEE Transactions on Geoscience and Remote Sensing, 2018, 56, 78-92.	2.7	10
136	The Webâ€Based Interactive Mars Analysis and Research System for HRSC and the iMars Project. Earth and Space Science, 2018, 5, 308-323.	1.1	10
137	MADNet 2.0: Pixel-Scale Topography Retrieval from Single-View Orbital Imagery of Mars Using Deep Learning. Remote Sensing, 2021, 13, 4220.	1.8	10
138	ExoMars Rover PanCam: Autonomous & Computational Intelligence [Application Notes]. IEEE Computational Intelligence Magazine, 2013, 8, 52-61.	3.4	9
139	Sensor Intercalibration Over Dome C for the ESA GlobAlbedo Project. IEEE Transactions on Geoscience and Remote Sensing, 2013, 51, 1139-1146.	2.7	9
140	Matching of Large Images Through Coupled Decomposition. IEEE Transactions on Image Processing, 2015, 24, 2124-2139.	6.0	9
141	Synergy of stereo cloud top height and ORAC optimal estimation cloud retrieval: evaluation and application to AATSR. Atmospheric Measurement Techniques, 2016, 9, 909-928.	1.2	9
142	Assessment of Satellite-Derived Surface Reflectances by NASA's CAR Airborne Radiometer over Railroad Valley Playa. Remote Sensing, 2017, 9, 562.	1.8	9
143	Automatic Coregistration and orthorectification (ACRO) and subsequent mosaicing of NASA high-resolution imagery over the Mars MC11 quadrangle, using HRSC as a baseline. Planetary and Space Science, 2018, 151, 33-42.	0.9	9
144	Super-Resolution Restoration of Spaceborne Ultra-High-Resolution Images Using the UCL OpTiGAN System. Remote Sensing, 2021, 13, 2269.	1.8	9

#	Article	IF	CITATIONS
145	Building Extraction Building Extraction and Verification from Spaceborne and Aerial Imagery using Image Understanding Fusion Techniques. , 1995, , 221-230.		9
146	The Western Elysium Planitia Paleolake. , 2010, , 275-305.		8
147	Comparing experts and novices in Martian surface feature change detection and identification. International Journal of Applied Earth Observation and Geoinformation, 2018, 64, 354-364.	1.4	8
148	Simulating Multi-Directional Narrowband Reflectance of the Earth's Surface Using ADAM (A Surface) Tj ETQq0	0 0 0 rgBT 1.8	/Qverlock 10
149	Subsurface Reflectors Detected by SHARAD Reveal Stratigraphy and Buried Channels Over Central Elysium Planitia, Mars. Earth and Space Science, 2021, 8, e2019EA000968.	1.1	8
150	Seamless 3D Image Mapping and Mosaicing of Valles Marineris on Mars Using Orbital HRSC Stereo and Panchromatic Images. Remote Sensing, 2021, 13, 1385.	1.8	8
151	Large Area High-Resolution 3D Mapping of Oxia Planum: The Landing Site for the ExoMars Rosalind Franklin Rover. Remote Sensing, 2021, 13, 3270.	1.8	8
152	Global albedo, BRDF and nadir BRDF-adjusted reflectance products from MODIS. , 0, , .		7
153	Assessment of multispectral ATSR2 stereo cloud-top height retrievals. Remote Sensing of Environment, 2006, 104, 337-345.	4.6	7
154	Crack Detection in "As-Cast" Steel Using Laser Triangulation and Machine Learning. , 2016, , .		7
155	Monitoring Land Subsidence in a Rural Area Using a Combination of ADInSAR and Polarimetric Coherence Optimization. IEEE Journal of Selected Topics in Applied Earth Observations and Remote Sensing, 2017, 10, 3582-3590.	2.3	7
156	Qualityâ€assured longâ€ŧerm satelliteâ€based leaf area index product. Global Change Biology, 2017, 23, 5027-5028.	4.2	7
157	MERIS observations of phytoplankton phenology in the Baltic Sea. Science of the Total Environment, 2018, 642, 447-462.	3.9	7
158	The 2016 UK Space Agency Mars Utah Rover Field Investigation (MURFI). Planetary and Space Science, 2019, 165, 31-56.	0.9	7
159	Towards Streamlined Single-Image Super-Resolution: Demonstration with 10 m Sentinel-2 Colour and 10–60 m Multi-Spectral VNIR and SWIR Bands. Remote Sensing, 2021, 13, 2614.	1.8	7
160	Assessment of the Performance of the Chilbolton 3-GHz Advanced Meteorological Radar for Cloud-Top-Height Retrieval. Journal of Applied Meteorology and Climatology, 2005, 44, 876-887.	1.7	6
161	The EU LOUDMAP project: Cirrus and contrail cloudâ€top maps from satellites for weather forecasting climate change analysis. International Journal of Remote Sensing, 2007, 28, 1915-1919.	1.3	6
162	WindCam and MSPI: two cloud and aerosol instrument concepts derived from Terra/MISR heritage. Proceedings of SPIE, 2008, , .	0.8	6

#	Article	IF	CITATIONS
163	A search for polycyclic aromatic hydrocarbons over the Martian South Polar Residual Cap. Icarus, 2018, 308, 61-70.	1.1	6
164	A Multi-Annotator Survey of Sub-km Craters on Mars. Data, 2020, 5, 70.	1.2	6
165	Automatic Seed Point Generation For Stereo Matching And Multi-image Registration. , 0, , .		5
166	Combination of Persistent Scatterer Interferometry and Single-Baseline Polarimetric Coherence Optimisation to Estimate Deformation Rates with Application to Tehran Basin. PFG - Journal of Photogrammetry, Remote Sensing and Geoinformation Science, 2017, 85, 327-340.	0.7	5
167	Automated reconstruction of subsurface interfaces in Promethei Lingula near the Martian south pole by using SHARAD data. Planetary and Space Science, 2019, 166, 59-69.	0.9	5
168	Application Of Ray-tracing to Satellite Image Understanding. , 0, , .		4
169	Botanical Plant Modelling For Remote Sensing Simulation Studies. , 0, , .		4
170	Global Topography Accuracy Requirements For EOS. , 0, , .		4
171	GROUND CONTROL DETERMINATION FOR REGISTRATION OF SATELLITE IMAGERY USING DIGITAL MAP DATA. Photogrammetric Record, 2006, 12, 809-822.	0.4	4
172	Epifluorescence surveys of extreme environments using PanCam imaging systems: Antarctica and the Mars regolith. Proceedings of SPIE, 2008, , .	0.8	4
173	The efficacy of satellite information in improving CMAQ/Models-3 prediction of ozone episodes in the US–Mexico border. Air Quality, Atmosphere and Health, 2010, 3, 159-169.	1.5	4
174	Multi-resolution digital terrain models and their potential for Mars landing site assessments. Planetary and Space Science, 2013, 85, 89-105.	0.9	4
175	Global warping coefficients for improving ATSR co-registration. Remote Sensing Letters, 2013, 4, 151-160.	0.6	4
176	Information content analysis: the potential for methane isotopologue retrieval from GOSAT-2. Atmospheric Measurement Techniques, 2018, 11, 1159-1179.	1.2	4
177	Influences of leaf area index and albedo on estimating energy fluxes with HOLAPS framework. Journal of Hydrology, 2020, 580, 124245.	2.3	4
178	Landslide Susceptibility Mapping Using GIS-based Vector Grid File (VGF) Validating with InSAR Techniques: Three Gorges, Yangtze River (China). AIMS Geosciences, 2017, 3, 116-141.	0.4	4
179	ENHANCEMENT OF STEREO IMAGERY BY ARTIFICIAL TEXTURE PROJECTION GENERATED USING A LIDAR. International Archives of the Photogrammetry, Remote Sensing and Spatial Information Sciences - ISPRS Archives, 0, XLI-B5, 599-606.	0.2	4
180	DATA FUSION OF LIDAR INTO A REGION GROWING STEREO ALGORITHM. International Archives of the Photogrammetry, Remote Sensing and Spatial Information Sciences - ISPRS Archives, 0, XL-4/W5, 107-112.	0.2	4

#	Article	IF	CITATIONS
181	Measurement Of Surface Microtopography Using Helicopter-mounted Stereo Film Cameras And Two Stereo Matching Techniques. , 0, , .		3
182	Real-time Stereo Matching Spot Using Transputer Arrays. , 0, , .		3
183	Surface Roughness Estimation Using Fractal Variogram Analysis. , 0, , .		3
184	Derivation of a global land elevation data set from satellite radar altimeter data for topographic mapping. Journal of Geophysical Research, 1998, 103, 32159-32168.	3.3	3
185	An evaluation of global urban growth via comparison of DCW and DMSP-OLS satellite data. , 0, , .		3
186	Mapping urban landcover using the bidirectional reflectance distribution function BRDF/albedo product from the Moderate Resolution Imaging Spectroradiometer (MODIS). , 0, , .		3
187	Ten years of MISR observations from Terra: Looking back, ahead, and in between. , 2010, , .		3
188	Contemporaneous Monitoring of the Whole Dynamic Earth System from Space, Part I: System Simulation Study Using GEO and Molniya Orbits. Remote Sensing, 2021, 13, 878.	1.8	3
189	EU-FP7-iMARS: ANALYSIS OF MARS MULTI-RESOLUTION IMAGES USING AUTO-COREGISTRATION, DATA MINING AND CROWD SOURCE TECHNIQUES: PROCESSED RESULTS $\hat{a} \in \mathcal{A}$ FIRST LOOK. International Archives of the Photogrammetry, Remote Sensing and Spatial Information Sciences - ISPRS Archives, 0, XLI-B4, 453-458.	0.2	3
190	3D Data Products and Web-GIS for Mars Rover Mission for Seamless Visualisation from Orbit to Ground-level. International Archives of the Photogrammetry, Remote Sensing and Spatial Information Sciences - ISPRS Archives, 0, XL-4, 249-256.	0.2	3
191	ICESAT VALIDATION OF TANDEM-X I-DEMS OVER THE UK. International Archives of the Photogrammetry, Remote Sensing and Spatial Information Sciences - ISPRS Archives, 0, XLI-B4, 129-136.	0.2	3
192	FLUORESCENT ANALYSIS OF PHOTOSYNTHETIC MICROBES AND POLYCYCLIC AROMATIC HYDROCARBONS LINKED TO OPTICAL REMOTE SENSING. International Archives of the Photogrammetry, Remote Sensing and Spatial Information Sciences - ISPRS Archives, 0, XXXIX-B8, 555-559.	0.2	3
193	Subpixel-Scale Topography Retrieval of Mars Using Single-Image DTM Estimation and Super-Resolution Restoration. Remote Sensing, 2022, 14, 257.	1.8	3
194	Estimating land surface albedo in the HAPEX-Sahel experiment: model-based inversions using ASAS. , 0, , . \cdot		2
195	Integrated field testing of planetary robotics vision processing: the PRoVisG campaign in Tenerife 2011. Proceedings of SPIE, 2012, , .	0.8	2
196	Calibrating Mars Orbiter Laser Altimeter pulse widths at Mars Science Laboratory candidate landing sites. Planetary and Space Science, 2014, 99, 118-127.	0.9	2
197	Repeat multiview panchromatic super-resolution restoration using the UCL MAGiGAN system. , 2018, , .		2
198	QUANTITATIVE ASSESSMENT OF A NOVEL SUPER-RESOLUTION RESTORATION TECHNIQUE USING HIRISE WITH NAVCAM IMAGES: HOW MUCH RESOLUTION ENHANCEMENT IS POSSIBLE FROM REPEAT-PASS OBSERVATIONS. International Archives of the Photogrammetry, Remote Sensing and Spatial Information Sciences - ISPRS Archives, 0, XLI-B4, 503-509.	0.2	2

#	Article	IF	CITATIONS
199	Assessment of the Effects of Resolution on Automated DEM and Building Extraction. , 1997, , 233-242.		2
200	Spot Dem Shading For Landsat-tm Topographic correction. , 0, , .		1
201	Global change video: visualization freeze-frames. IEEE Computer Graphics and Applications, 1993, 13, 11-13.	1.0	1
202	Investigations of the spatial variability of albedo during the Grassland PROVE '97 Jornada field campaign. , 1998, , .		1
203	Correction to "Late Noachian to Hesperian climate change on Mars: Evidence of episodic warming from transient crater lakes near Ares Vallis― Journal of Geophysical Research, 2011, 116, .	3.3	1
204	A simple and quick sensitivity analysis method for methane isotopologues detection with GOSAT-TANSO-FTS. UCL Open Environment, 0, 2, .	0.0	1
205	3D MULTI-RESOLUTION MAPPING OF MARS USING CASP-GO ON HRSC, CRISM, CTX AND HIRISE. International Archives of the Photogrammetry, Remote Sensing and Spatial Information Sciences - ISPRS Archives, 0, XLIII-B3-2021, 667-671.	0.2	1
206	The Detectability Limit of Organic Molecules Within Mars South Polar Laboratory Analogs. Journal of Geophysical Research E: Planets, 2021, 126, e2020JE006595.	1.5	1
207	Reservoir Monitoring Using Satellite SAR and GNSS: a Case Study in Southern Italy. , 0, , .		1
208	IDENTIFYING SURFACE CHANGES ON HRSC IMAGES OF THE MARS SOUTH POLAR RESIDUAL CAP (SPRC). International Archives of the Photogrammetry, Remote Sensing and Spatial Information Sciences - ISPRS Archives, 0, XLI-B4, 463-469.	0.2	1
209	IR SPECTRAL MAPPING OF THE MARTIAN SOUTH POLAR RESIDUAL CAP USING CRISM. International Archives of the Photogrammetry, Remote Sensing and Spatial Information Sciences - ISPRS Archives, 0, XLI-B7, 71-75.	0.2	1
210	AN OPTIMISED SYSTEM FOR GENERATING MULTI-RESOLUTION DTMS USING NASA MRO DATASETS. International Archives of the Photogrammetry, Remote Sensing and Spatial Information Sciences - ISPRS Archives, 0, XLI-B3, 115-121.	0.2	1
211	EU-FP7-iMARS: ANALYSIS OF MARS MULTI-RESOLUTION IMAGES USING AUTO-COREGISTRATION, DATA MINING AND CROWD SOURCE TECHNIQUES: PROCESSED RESULTS & amp;ndash; A FIRST LOOK. International Archives of the Photogrammetry, Remote Sensing and Spatial Information Sciences - ISPRS Archives, 0, XLI-B4, 453-458.	0.2	1
212	EXTRACTION OF ICE SHEET LAYERS FROM TWO INTERSECTED RADAR ECHOGRAMS NEAR NEEM ICE CORE IN GREENLAND. International Archives of the Photogrammetry, Remote Sensing and Spatial Information Sciences - ISPRS Archives, 0, XLI-B7, 585-591.	0.2	1
213	STEREO DERIVED CLOUD TOP HEIGHT CLIMATOLOGY OVER GREENLAND FROM 20 YEARS OF THE ALONG TRACK SCANNING RADIOMETER (ATSR) INSTRUMENTS. International Archives of the Photogrammetry, Remote Sensing and Spatial Information Sciences - ISPRS Archives, 0, XXXIX-B8, 109-113.	0.2	1
214	Cornea shape measurement. , 1990, , .		1
215	BATCH CO-REGISTRATION OF MARS HIGH-RESOLUTION IMAGES TO HRSC MC11-E MOSAIC. International Archives of the Photogrammetry, Remote Sensing and Spatial Information Sciences - ISPRS Archives, 0, XLI-B4, 491-495.	0.2	1
216	The Moderate Resolution Imaging Spectroradiometer (MODIS) BRDF and albedo product: preliminary results. , 0, , .		1

Jan Peter Muller

#	Article	IF	CITATIONS
217	SEnSel: A Deep Learning Module for Creating Sensor Independent Cloud Masks. IEEE Transactions on Geoscience and Remote Sensing, 2022, 60, 1-21.	2.7	1
218	MODIS operational bidirectional reflectance and albedo products. , 0, , .		0
219	Correction [to "Measurements of wind vectors, eddy momentum transports, and energy conversions in Jupitor's atmosphere from Voyager 1 imagesâ€]. Geophysical Research Letters, 1980, 7, 621-622.	1.5	Ο
220	At-launch status of the MODIS BRDF/albedo algorithm: implementation, AVHRR-based prototyping, and future plans. , 1998, , .		0
221	High resolution interferometric SAR DEMs for hydrological network derivation. , 0, , .		0
222	An application of stereomatching to the problem of geo-referencing historical air-photos. , 0, , .		0
223	Extracting Tree Heights over Topography with Multi-Spectral Spaceborne Waveform Lidar. , 2008, , .		0
224	Global analysis of the improvements in AATSR nadir-forward co-registration following the application of an automated registration algorithm. , 2012, , .		0
225	Exploiting ten years of MERIS data over land surfaces. , 2012, , .		0
226	Satellite sensor intercalibration over Dome C: An introduction to QA4EO and the ESA GlobAlbedo project. , 2012, , .		0
227	XXIInd International Congress of Photogrammetry and Remote Sensing. Photogrammetric Record, 2013, 28, 43-73.	0.4	0
228	Development of robust quality assurance procedures for terrestrial essential climate variable data products derived from Earth Observation satellites. , 2016, , .		0
229	In-Situ and Aircraft Reflectance Measurement Effectiveness for CAL/VAL Activities: A Study over Railroad Valley. Remote Sensing, 2020, 12, 3366.	1.8	0
230	A Method of Retrieving 10-m Spectral Surface Albedo Products from Sentinel-2 and MODIS data. , 2021, ,		0
231	InSAR measurement of fault activity in Red River fault zone. , 2010, , 747-750.		0
232	Temporal analysis of all high-resolution Mars imaging products. International Archives of the Photogrammetry, Remote Sensing and Spatial Information Sciences - ISPRS Archives, 0, XL-4, 235-238.	0.2	0
233	An Improved Baseline Estimation Method using External DEMS in Different Terrain Areas. , 2015, , .		0
234	Extraction of Subsurface Features from InSAR-derived Digital Elevation Models. , 2015, , .		0

14

#	Article	IF	CITATIONS
235	IR SPECTRAL MAPPING OF THE MARTIAN SOUTH POLAR RESIDUAL CAP USING CRISM. International Archives of the Photogrammetry, Remote Sensing and Spatial Information Sciences - ISPRS Archives, 0, XLI-B7, 71-75.	0.2	0
236	IDENTIFYING SURFACE CHANGES ON HRSC IMAGES OF THE MARS SOUTH POLAR RESIDUAL CAP (SPRC). International Archives of the Photogrammetry, Remote Sensing and Spatial Information Sciences - ISPRS Archives, 0, XLI-B4, 463-469.	0.2	0
237	EVALUATION OF THE MAIN CEOS PSEUDO CALIBRATION SITES USING MODIS BRDF/ALBEDO PRODUCTS. International Archives of the Photogrammetry, Remote Sensing and Spatial Information Sciences - ISPRS Archives, 0, XLI-B1, 217-220.	0.2	0
238	EXTRACTION OF ICE SHEET LAYERS FROM TWO INTERSECTED RADAR ECHOGRAMS NEAR NEEM ICE CORE IN GREENLAND. International Archives of the Photogrammetry, Remote Sensing and Spatial Information Sciences - ISPRS Archives, 0, XLI-B7, 585-591.	0.2	0
239	QUANTITATIVE ASSESSMENT OF A NOVEL SUPER-RESOLUTION RESTORATION TECHNIQUE USING HIRISE WITH NAVCAM IMAGES: HOW MUCH RESOLUTION ENHANCEMENT IS POSSIBLE FROM REPEAT-PASS OBSERVATIONS. International Archives of the Photogrammetry, Remote Sensing and Spatial Information Sciences - ISPRS Archives. 0. XLI-B4. 503-509.	0.2	0
240	Performance of global 3D model retrievals of the Martian surface using the UCL CASP-GO system on CTX stereo images on linux clusters and Microsoft Azure® cloud computing platforms. , 2018, , .		0